Impaired Extraocular Muscle Innervation Is Present Before Eye Opening in a Mouse Model of Infantile Nystagmus Syndrome

Sampath Kumar Vemula,[1] Seoyoung A. Kim,[1] Tapiwa Muvavarirwa,[1] Jessica L. Bell,[1,*] and Mary C. Whitman[1–3]

[1]Department of Ophthalmology, Boston Children's Hospital, Boston, Massachusetts, United States
[2]Department of Ophthalmology, Harvard Medical School, Boston, Massachusetts, United States
[3]F.M. Kirby Neurobiology Center, Boston Children's Hospital, Boston, Massachusetts, United States

Correspondence: Mary C. Whitman, Department of Ophthalmology, Boston Children's Hospital, 3 Blackfan Circle, CLS 18042, Boston, MA 02115, USA; mary.whitman@childrens.harvard.edu.

Current affiliation: *Department of Genetics and Neuroscience Center, University of North Carolina at Chapel Hill, Chapel Hill, North Carolina, United States.

Received: July 1, 2022
Accepted: August 20, 2022
Published: September 9, 2022

Citation: Vemula SK, Kim SA, Muvavarirwa T, Bell JL, Whitman MC. Impaired extraocular muscle innervation is present before eye opening in a mouse model of infantile nystagmus syndrome. *Invest Ophthalmol Vis Sci.* 2022;63(10):4. https://doi.org/10.1167/iovs.63.10.4

Purpose. To determine if extraocular muscles (EOMs) from mice with nystagmus show abnormalities in myofiber composition and innervation, as seen in EOMs from human nystagmus patients, and to determine when in development those changes occur.

Methods. Balb/c albino mice were crossed to pigmented mice to generate heterozygous mice, which were mated to create experimental litters containing albinos and wild-type controls. Orbits were harvested from adult animals (12 weeks old); on postnatal day (P)0, P10, P14, and P21; and from 6-week-old animals. EOM sections were collected from the intraorbital portion of the muscles. Sections were immunostained for slow and fast myosin and for neuromuscular junctions (NMJs). The proportion of each myofiber subtype and the density and size of NMJs were quantified. Initial innervation patterns were assessed using whole-mount immunostaining of embryonic day (E)13.5 embryos expressing *Isl^{MN}:GFP*.

Results. Adult albino EOMs display an increased proportion of slow myofibers, larger slow myofibers, and a decreased density of NMJs—similar to human nystagmus patients. The percentage of NMJs on slow myofibers is also lower in albino animals. The initial innervation pattern of the incoming ocular motor neurons is normal in E13.5 albino embryos. Differences in the proportion of slow and fast myofiber subtypes are present as early as P14, and a lower percentage of NMJs on slow myofibers is present by P21. There is a lower density of NMJs on albino EOMs as early as P10, prior to eye opening.

Conclusions. Changes in NMJ development observed before eye opening indicate that nystagmus is not solely secondary to poor vision.

Keywords: nystagmus, neuromuscular junction, albinism, development, extraocular muscle

Nystagmus is an involuntary, rhythmic oscillation of one or both eyes, often characterized by an initial slow movement followed by a fast, jerk refixation movement. Infantile nystagmus syndrome (INS) begins before 6 months of age, affects approximately one in 800 children,[1] and is often accompanied by conditions involving afferent visual deficits such as optic nerve hypoplasia, aniridia, retinal dystrophies, or albinism.[1–3] Eye movements are coordinated by six extraocular muscles (EOMs), which are innervated by three cranial motor nerves.[4] The EOMs are a unique muscle group based on their molecular composition and function.[5] They are composed of several different myofiber types, which express different types of myosin heavy chains (MyHCs). The simplest way to classify them is to divide them into two broad categories (slow and fast) based on the type of MyHC they express. Fast myofibers have one concentrated area of motor endplates where they receive neuromuscular junctions (NMJs) from fast-firing ocular motor neurons (OMNs) and are thus known as singly innervated fibers (SIFs).[6,7] Slow myofibers, in contrast, are multiply innervated fibers (MIFs) exhibiting multiple motor endplates from slow-firing OMNs along the length of one fiber. The slow and fast subtypes of OMNs originate from different areas of the cranial motor nuclei and have different premotor inputs. It has thus been proposed that SIF and MIF motor neurons control distinct types of eye movements,[8,9] but recent recordings from cats indicate that both motor neuron types contribute to all types of eye movements, although with differing physiologic properties, indicating that they may serve different functions.[10,11]

Studies of EOMs from human nystagmus patients (taken during eye muscle surgery) show evidence of decreased innervation; nerve fiber density, mean myelinated nerve density, NMJ area, and NMJ density are all decreased. In addition, the number and size of slow myosin fibers are increased.[12,13] The EOMs of patients with nystagmus also exhibited a 10-fold increase in levels of central nucleation, consistent with cycles of degeneration and regeneration.[12]

Copyright 2022 The Authors

This work is licensed under a Creative Commons Attribution-NonCommercial-NoDerivatives 4.0 International License.

Downloaded from intl.iovs.org on 04/26/2024

However, these EOM specimens were taken years after the onset of nystagmus,[12,13] so it cannot be determined whether these changes are the cause or the result of INS. In order to study the development of these changes, we propose the use of Balb/c albino mice as a model to study development of nystagmus.[14]

The albino Balb/c mouse strain (and other albino strains) displays spontaneous nystagmus and an abnormal optokinetic response when viewing a moving grating, making this mouse a good animal model for nystagmus.[14] Our aim was to determine whether albino mice recapitulate the changes seen in human nystagmus EOMs and then to determine when in development these changes are first evident. We compared muscle fiber composition and NMJ development between control and albino mice EOMs and showed that albino mice do recapitulate the EOM phenotypes. We further show that decreases in NMJ density occur first, as early as postnatal day (P)10, before eye opening.

Materials and Methods

Animals

Balb/c albino mice (Jax 000651; *Tyr$^{c/c}$* point mutation in tyrosinase which eliminates enzyme function[15]) were crossed to transgenic wild-type *Isl^{MN}:GFP* reporter mice, which express farnesylated green fluorescent protein (GFP) in the membranes of motor neurons and axons, to visualize the nerves during development.[16] Mice that were heterozygous for albinism and expressed *Isl^{MN}:GFP* were crossed to each other to generate experimental litters that contained albino and wild-type littermate controls. The number of animals used at each age for each experiment is provided in the figure legends. All experiments were performed in compliance with the ARVO Statement for the Use of Animals in Ophthalmic and Vision Research and were approved by the Boston Children's Hospital Institutional Animal Care and Use Committee.

Tissue Collection and Processing

P0 and P10 mouse heads were collected and fixed overnight with freshly prepared 4% paraformaldehyde (PFA) (15710; Electron Microscopy Sciences, Hatfield, PA, USA) in phosphate-buffered saline (PBS; pH 7.4). P14 and older animals were anesthetized with ketamine/xylazine and transcardially perfused with 4% PFA in PBS. The heads were bisected, and orbits were collected. After overnight fixation with 4% PFA in PBS, the orbits were washed three times with PBS and were transferred to 30% sucrose solution until they sank. The orbits were frozen using NEG50 (6502; Epredia, Kalamazoo, MI, USA) in a cryomold (Tissue-Tek O.C.T. Compound, 4566; Sakura-Finetek, Torrance, CA, USA). Then, 20-µm sections were cut on a cryostat, oriented so the muscles were in cross section. We focused specifically on the lateral rectus (LR) and medial rectus (MR) muscles for this study, and all results are from those muscles.

Immunohistochemistry

Muscle sections were fixed with 4% PFA for 10 minutes at room temperature (RT) and washed three times with PBS at RT. Then, the sections were incubated with a blocking solution comprised of 2% normal goat serum in 0.2% Triton X-100 in PBS (PBS-T), for 1 hour at RT. They were incubated with a primary antibody, Anti-Myosin Antibody, slow muscle, clone NOQ7.5.4D (1:200, MAB1628; MilliporeSigma, Burlington, MA, USA) to detect slow myofibers. They were then soaked in blocking solution overnight at 4°C, washed three times with PBS-T, and incubated with fluorescent-conjugated anti-mouse Alexa Fluor 647 secondary antibody (1:1000; The Jackson Laboratory, West Grove, PA, USA) and washed with PBS-T. Then, to detect fast myofibers, the sections were blocked and incubated with a second antibody, Anti-Myosin (Skeletal, Fast) antibody, mouse monoclonal (1:300, M1570; Sigma-Aldrich, St. Louis, MO, USA), overnight at 4°C, washed, and incubated with fluorescent-conjugated anti-mouse Alexa Fluor 488 secondary antibody (1:1000; The Jackson Laboratory) and Invitrogen Alexa Fluor 594-conjugated α-Bungarotoxin (1:500, B13423; Thermo Fisher Scientific, Waltham, MA, USA) for 1 hour at RT to label acetylcholine receptors (AChRs). The sections were washed and mounted with Invitrogen Fluoromount-G (00-4958-02; Thermo Fisher Scientific). To ensure there was no cross-reactivity between the antibodies, the procedure was performed without the addition of the second primary antibody. In those cases, there was no staining of the second secondary antibody (not shown).

Hematoxylin and Eosin Staining

Sections were treated with hematoxylin solution (HHS16; Sigma-Aldrich) and rinsed in distilled water until the water was colorless. Sections were washed with tap water, dipped in 70% ethanol–hydrogen chloride, and washed with tap water and distilled water. Next, the sections were treated with eosin Y solution (HT110316; Sigma-Aldrich), rinsed in distilled water, dehydrated through an ethanol series, soaked with xylene, and mounted with Permount Mounting Medium (17986-01; Electron Microscopy Sciences). Central nuclei were counted by hand by an observer blinded to genotype.

Whole-Mount Immunostaining and Clearing of Tissue

Whole-mount immunostaining was performed on embryonic day (E)13.5 wild-type and albino *Isl^{MN}:GFP* mouse embryos (which express GFP in the motor neurons) using the iDisco+ method, as previously described.[17,18] Briefly, the embryos were fixed overnight in 4% PFA and dehydrated with a methanol series of 20%, 40%, 60%, 80%, and twice with 100% for 1 hour each at RT. Then, the embryos were bleached with 5% hydrogen peroxide in methanol overnight at 4°C, rehydrated with a methanol series in a reverse order, and further washed twice with PTx.2 solution (2% TritonX-100 in PBS). The embryos were transferred to permeabilization solution (20% dimethyl sulfoxide [DMSO] and 306-mM glycine in PTx.2 solution) and incubated at 37°C for 2 days on a rotating shaker. The embryos were then incubated with blocking solution (6% donkey serum and 10% DMSO in PTx.2 solution) for an additional 2 days at 37°C. They were then incubated with primary antibodies, including mouse anti-actin, α-smooth muscle-Cy3 (1:750; MilliporeSigma) and rabbit anti-GFP (1:500; Thermo Fisher Scientific), in a solution of 0.2% Tween-20 and heparin in PBS (PTwH), 5% DMSO, and 3% donkey serum for 7 days at 37°C. They were washed with PTwH for 1 day at RT and incubated with a secondary antibody, rabbit anti-GFP-Alexa Fluor 647

Investigative Ophthalmology & Visual Science

Downloaded from intl.iovs.org on 04/26/2024

(1:500; Thermo Fisher Scientific), diluted in a solution of PTwH with 3% donkey serum, for 7 days at 37°C. They were washed with PTwH solution for 1 day at RT. For clearing, the embryos were dehydrated with a methanol series and incubated with a solution of 66% dichloromethane (Sigma-Aldrich) and 33% methanol (Sigma-Aldrich) for 3 hours at RT. Finally, the embryos were transferred to dibenzyl ether solution (Sigma-Aldrich) for imaging.

Image Acquisition and Analysis

Whole-mount embryos were mounted with coverslips in a special chamber with dibenzyl ether and imaged using an inverted Zeiss LSM 710 laser scanning confocal microscope (Carl Zeiss MicroImaging GmbH, Gottingen, Germany). Images were acquired using Zeiss ZEN software and viewed and quantified in three dimensions using Imaris software (Bitplane, Zurich, Switzerland). The diameter of CN3 was measured at four different points: before entering the orbit and before making a branch on the superior rectus (SR), MR, and inferior oblique (IO).

The muscle sections were imaged using the Zeiss LSM 710 microscope. All images were quantified by an examiner blinded to genotype. Total myofiber number and slow and fast MyHC-positive myofibers were quantified for each image, and the percentages of slow and fast myofibers were calculated. We imaged every fifth section along 500 to 700 µm of muscle length, comprised of the portion of muscle from the posterior edge of the eyeball to the muscle origin. Using Fiji for ImageJ (National Institutes of Health, Bethesda, MD, USA) with a particle size analyzer tool, we quantified the mean cross-sectional area of slow muscle fibers, as well as the number, size, and average area of NMJs, for each muscle. We also calculated the percentage of NMJs on slow myofibers.

Statistical Analysis

Statistical analysis of all raw data was performed using Prism 9 (GraphPad, San Diego, CA, USA). All data on the graphs are represented as mean ± standard error of the mean (SEM). Data presented in the text are reported as mean ± standard deviation (SD). Student's *t*-test was performed to compare the data between genotypes in adults. To compare across age and genotypes, two-way ANOVA was performed followed by Sidak's multiple comparisons testing.

Results

Albino Mice EOMs Recapitulate the Phenotype Seen in Human Nystagmus EOMs

To determine whether the changes seen in nystagmus patients' EOMs are also present in albino mice, we quantified the proportion of slow and fast MyHC-expressing fibers in EOMs of 12-week-old albino mice and littermate controls. In control EOMs, fast MyHC was expressed in the majority of the myofibers, and slow MyHC was expressed in 14.1% ± 2.1% of myofibers (Fig. 1A). In albino EOMs, the percentage of slow myofibers was significantly higher (20.0% ± 2.6%; $P = 0.0013$) (Figs. 1B, 1C), and, consequently, fast myofibers were significantly reduced in albino EOMs (Fig. 1D). The slow myofiber cross-sectional area was increased in EOMs of albinos compared with littermate controls (189.4 vs. 159.8 µm^2; $P = 0.03$) (Fig. 1E). The total number of myofibers was not significantly different (320.7 ± 33.2 vs. 273.8 ± 13.6; $P = 0.22$), nor was the total muscle area (113884 ± 3231 vs. 112766 ± 7622 µm^2; $P > 0.99$). We assessed for central nucleation of muscle fibers on hematoxylin and eosin (H&E)-stained tissue and found a significant increase in central nucleation in albinos (6.736% ± 1.02% vs. 3.351% ± 0.43%;

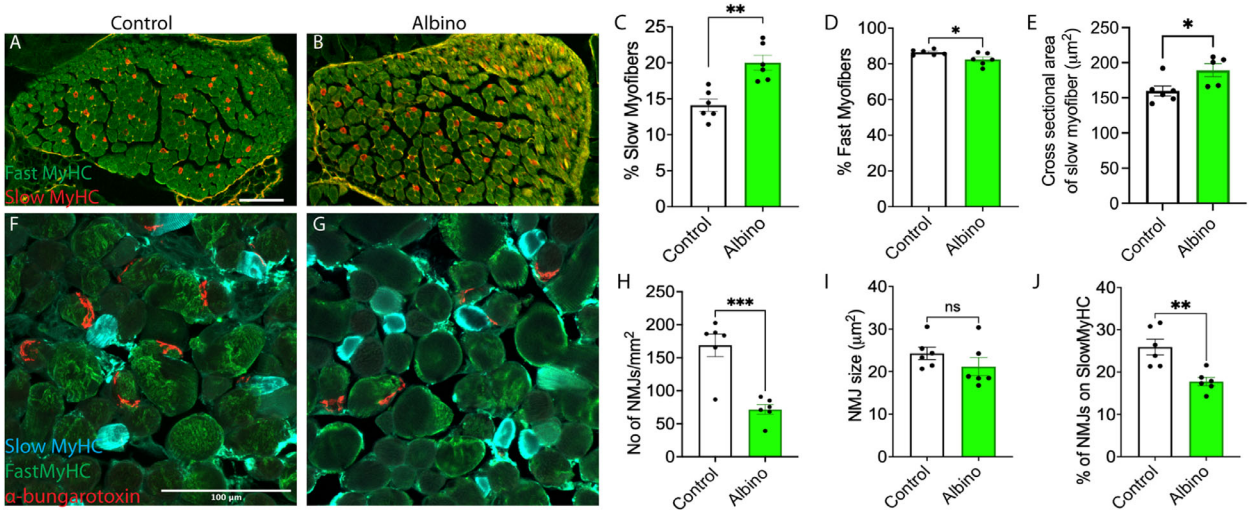

Figure 1. Slow and fast myosin expression in EOMs of adult albino and control mice. (**A**, **B**) Confocal images of LR muscles from 12-week-old albinos (**B**) and littermate controls (**A**) immunostained for fast MyHC (*green*) and slow MyHC (*red*). Images in **A** and **B** are from similar portions of the LR. (**C**) Quantification of the percentage of slow myofibers showed a significant increase in albinos compared with control muscles. (**D**) Quantification of the percentage of fast myofibers showed a significant decrease in albinos compared with controls. (**E**) Quantification of mean cross-sectional area of slow myofibers showed a significant increase in albinos. (**F**, **G**) Confocal images of control (**F**) and albino (**G**) LR immunostained for fast MyHC (*green*), slow MyHC (*cyan*), and acetylcholine receptors (α-bungarotoxin, *red*). Images in **F** and **G** are from similar portions of the LR. (**H**) NMJ density quantification showed a significant decrease in albinos compared with controls. (**I**) Average NMJ size did not differ between albinos and controls. (**J**) Analysis of the percentage of NMJs on slow myofibers showed a significant decrease in albinos. Data are represented as mean ± SEM. *$P < 0.05$, **$P < 0.001$, ***$P < 0.0001$ ($n = 6$ animals per genotype). *Scale bar*: 100 µm (**A**, **B**, **F**, **G**).

Investigative Ophthalmology & Visual Science

Downloaded from intl.iovs.org on 04/26/2024

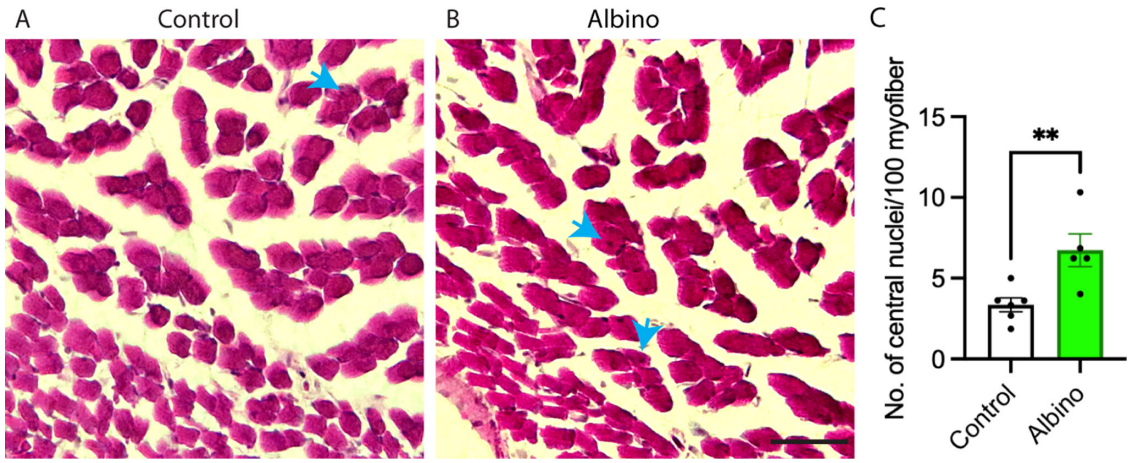

Figure 2. Increased central nucleation in albino EOMs. (**A**, **B**) Brightfield images of EOMs from 12-week-old albinos (**B**) and littermate controls (**A**) stained with H&E. *Blue arrows* indicate central nuclei. (**C**) Quantification of the percentage of myofibers with central nucleation showed a significant increase in albinos compared with control muscles. Data are represented as mean ± SEM. $^{**}P < 0.001$ (n = 5–6 animals per genotype). *Scale bar*: 100 µm.

$P = 0.0096$) (Fig. 2). We found that the density of NMJs was significantly reduced in EOMs of albinos compared to littermate controls (71.68 vs. 168.9 NMJs/mm^2; $P = 0.0004$) (Figs. 1F–1H). Furthermore, the percentage of NMJs on slow myofibers was significantly reduced in albinos (17.76% vs. 25.93%; $P = 0.003$) (Fig. 1J). The average size of NMJs did not differ between albino and control mice (21.2 vs. 24.3 µm^2; $P = 0.255$) (Fig. 1I). We analyzed each of these parameters in the LR and MR separately and obtained similar results (data not shown). These results indicate that albino mice show EOM and innervation changes similar to those seen in the EOMs of patients with nystagmus and can therefore be used to evaluate development of the oculomotor system in nystagmus.

Initial Embryonic Innervation of the EOMs Was Normal in Albinos

We next examined whether the initial routing of the OMNs to the EOMs is disturbed in albino mice. OMNs in the brainstem are born between E9.5 and E11.5 and extend axons toward the orbit beginning at E10.0, with branches to each EOM established by E13.5.[18–22] From heterozygous matings, we generated E13.5 litters with wild-type and albino embryos that express GFP in the motor neurons (*Isl^{MN}:GFP*) and prepared whole mounts. CN3, CN4, and CN6 axonal trajectories developed normally onto EOMs in albinos and in controls (Figs. 3A, 3B). To quantify the size of the nerve, the diameter of CN3 was measured at four different branch

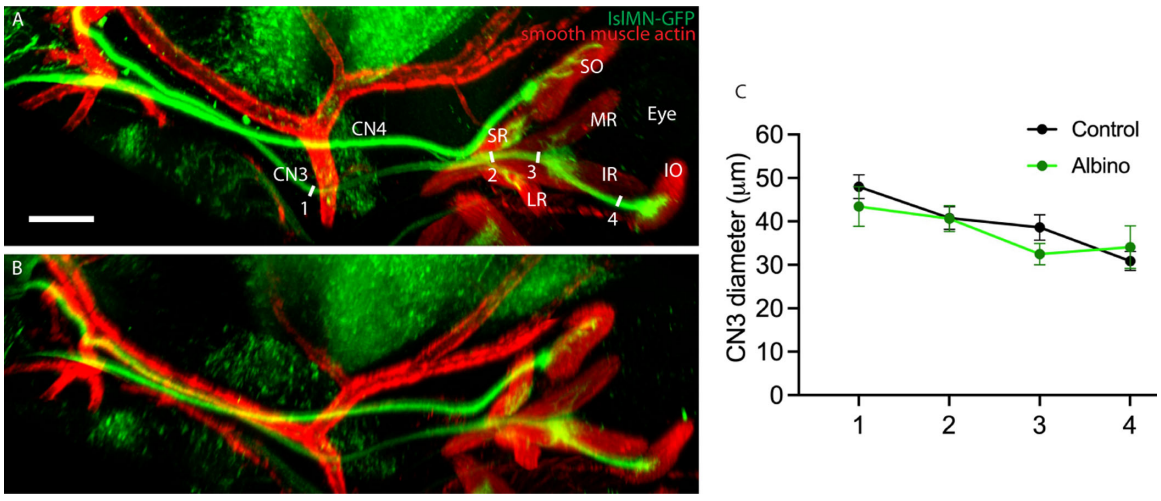

Figure 3. Initial motor neuron axon outgrowth was normal in E13.5 albino embryos. (**A**, **B**) Maximum intensity projections of whole-mount images from E13.5 wild-type (**A**) and albino (**B**) embryos. Lateral views into the orbit: midbrain is to the left, eye and orbit to the right. Motor neurons were genetically labeled with GFP under the *Isl1^{MN}* promoter (*green*), and muscles and arteries were labeled with anti-α-smooth muscle actin (*red*). In both albino and control embryos, CN3 axon trajectories are normal on the SR, MR, IR, and IO, and CN4 nerve axons are innervating the SO. The *green staining* superiorly in each image shows midline brain structures that also express *Isl^{MN}*:GFP (ectopically). *Scale bar*: 500 µm. (**C**) Quantification of CN3 diameter at four different points: near anterior carotid artery (1), before branching to SR (2), before branching to IR and MR (3), and branch to IO (4). These points are labeled on the control image (**A**). Data are represented as mean ± SEM (n = 7–13 embryos per genotype).

Investigative Ophthalmology & Visual Science

Downloaded from intl.iovs.org on 04/26/2024

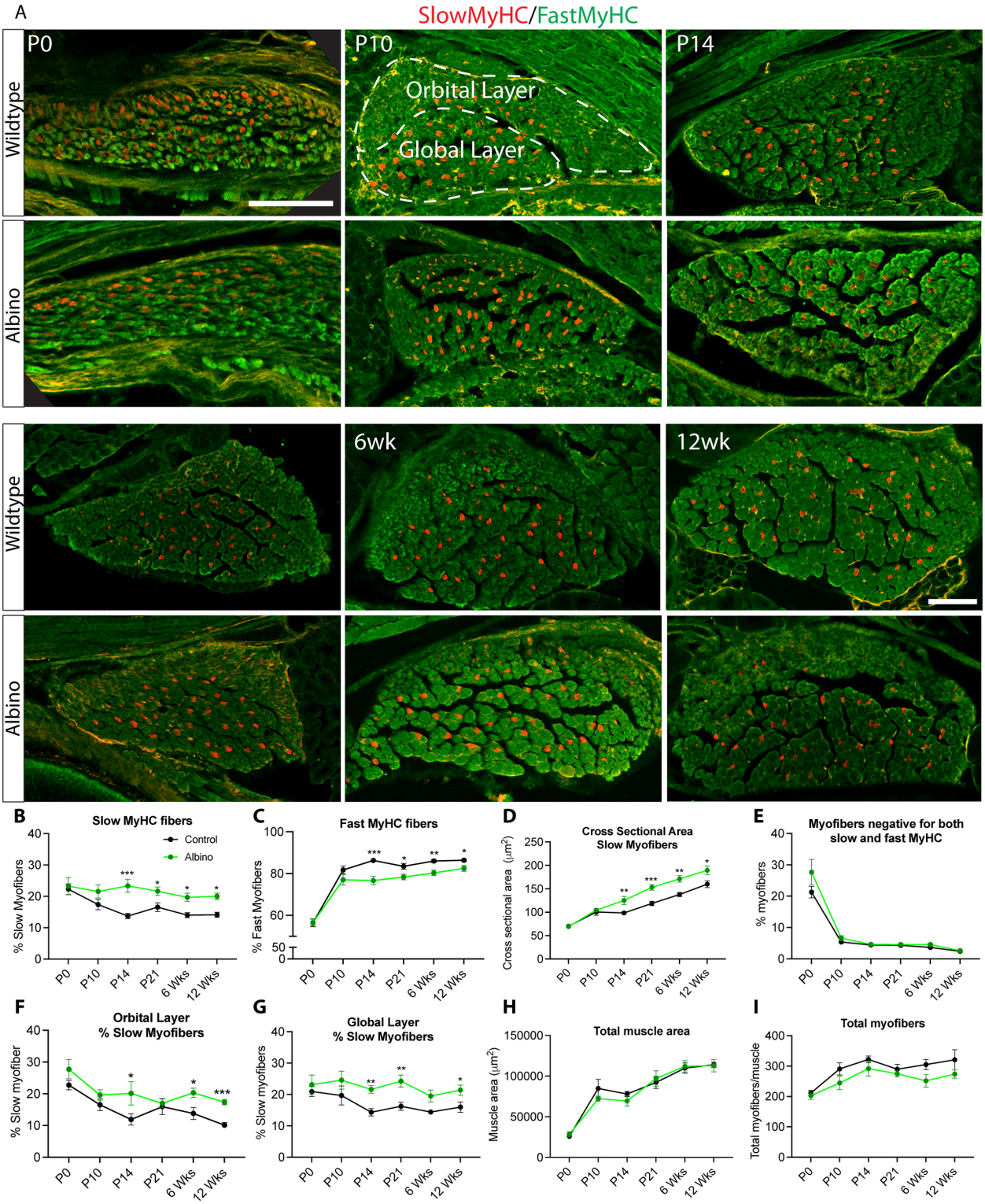

Figure 4. Differences in myofiber subtypes as early as P14. (**A**) EOM sections from P0, P10, P14, P21, 6-week-old, and 12-week-old control and albino mice were immunostained for slow (*red*) and fast (*green*) MyHC. Images at each time point are from similar portions of the muscle. The orbital and global layers are outlined on the P10 control image. (**B**, **C**) Quantification of the percentage of slow myofibers (**B**) and fast myofibers (**C**) showed significant differences from P14 to adulthood. (**D**) The slow myofiber cross-sectional area was significantly larger in albino EOMs from P14 to adulthood. (**E**) The percentage of myofibers not expressing fast or slow myosin was similar at all ages. (**F**, **G**) Albinos had an increased percentage of slow myofibers in both the orbital layer (**F**) and global layer (**G**), starting at P14. (**H**, **I**) The total muscle area and total number of myofibers were similar at all ages. *Scale bars*: 50 µm (P0) and 100 µm (P10–12 weeks). Data are represented as mean ± SEM (n = 5–10 animals per genotype at each time point). *P < 0.05, **P < 0.001, ***P < 0.0001.

Downloaded from intl.iovs.org on 04/26/2024

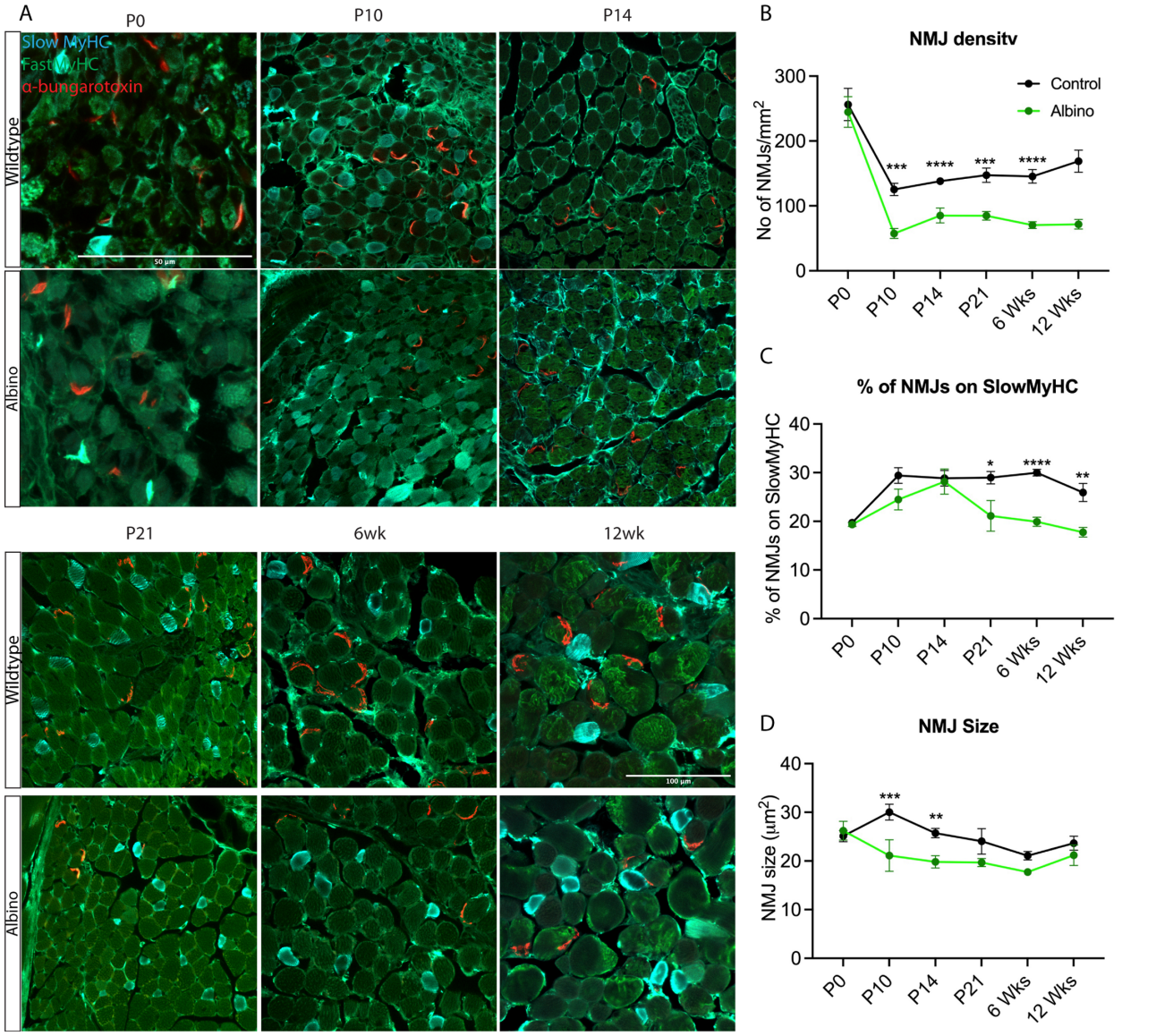

Figure 5. Differences in NMJ density and size first seen at P10. (**A**) EOM sections from P0, P10, P14, P21, 6-week-old, and 12-week-old control and albino mice were immunostained for slow MyHC (*cyan*), fast MyHC (*green*), and AChRs with α-bungarotoxin (*red*). (**B**) NMJ density was significantly lower in albinos from P10 through adulthood. (**C**) The percentage of NMJs on slow myofibers was lower in albinos starting at P21. (**D**) NMJ size increased transiently at P10 in wild-type animals, then decreased. This increase was not seen in albinos, leading to significant differences in NMJ size at P10 and P14 but not at other ages. *Scale bars*: 50 µm (P0) and 100 µm (P10–12 weeks). Data are represented as mean ± SEM (n = 5–10 animals per genotype at each time point). *$P < 0.05$, **$P < 0.001$, ***$P < 0.0001$, ****$P < 0.00001$.

points, and we found no difference between the controls and albinos (Fig. 3C), suggesting that early motor neuron axonal growth was normal in albino mice.

Slow and Fast Muscle Fiber Proportion Differences as Early as P14

To investigate when in development EOM changes first occur, we examined slow and fast MyHC expression in EOM sections covering the entire muscle length from P0, P10, P14, P21, 6-week-old, and 12-week-old albino and littermate control mice. In wild-type mice at P0, 22.3% ± 4.5% of the myofibers were slow myofibers. The proportion of slow myofibers decreased from P0 to P14 and then remained steady into adulthood (Figs. 4A, 4B). Similar results were observed in both the MR and LR (data not shown). In albino EOMs at P0, the proportion of slow myofibers (23.2% ± 7.7%) was similar to that of controls, but the proportion of slow myofibers remained relatively constant from P0 to adulthood, without the decrease seen between P0 and P14 in controls. This led to significant differences between albinos and controls at P14, P21, 6 weeks, and 12 weeks (Figs. 4A, 4B). Conversely, in controls, the proportion of fast myofibers increased gradually from P0 until P14 and then became stable. In albinos, the proportion of fast myofibers was similar to that of controls at P0. There was an increase in the proportion of fast myofibers from P0 to P14, but it was slower than that seen in controls (Fig. 4C). These results are consistent with published data indicating that slow

Investigative Ophthalmology & Visual Science

Downloaded from intl.iovs.org on 04/26/2024

MyHC-positive myofibers are expressed at high levels at birth and decrease gradually.[23] We also quantified the percentage of myofibers that express neither fast nor slow myosin at each age and found no differences between the genotypes (Fig. 4E). We examined the orbital and global layers of the muscle separately at each age and found that both layers showed an increased percentage of slow myofibers starting at P14 (Figs. 4F, 4G).

We next examined the cross-sectional area of the slow myofibers. At P0, slow myofibers were similar in size between controls and albinos (70.0 ± 8.3 vs. 69.4 ± 5.8 μm^2). There was a gradual increase in size of slow myofibers from P0 to adulthood in controls. The increase was faster in albinos, leading to significantly larger slow myofibers in albinos from P14 until adulthood (Fig. 4D). Total EOM muscle area did not differ at any age (Fig. 4H). The total numbers of myofibers were also similar (Fig. 4I). Two-way ANOVA showed a significant effect of both age and genotype, but at no age were the results significant after multiple comparisons testing.

Neuromuscular Junction Density Was Reduced as Early as P10

We next examined NMJs in EOMs of P0, P10, P14, P21, 6-week-old, and 12-week-old albinos and littermates. We examined sections along the entire muscle length and quantified those in which NMJs were present. In control mice, there was a sharp reduction in NMJ density between P0 and P10, after which it remained relatively stable. In albino mice, however, there was an even sharper reduction between P0 and P10, and NMJ density remained significantly lower at all older ages (Figs. 5A, 5B).

Neuromuscular Junction Loss Higher on Slow Myofibers

In control mice, there was an increase in the percentage of NMJs on slow myofibers from P0 to P10 and then steady levels to adulthood. In albino mice, however, the percentage of NMJs on slow myofibers was similar to controls until P14 but then decreased and was significantly lower than controls at P21, 6 weeks, and 12 weeks (Figs. 5A, 5C). The albino mice had an increased proportion of slow myofibers, but fewer of the NMJs were on slow myofibers and there was a lower density of NMJs overall, indicating that there was a particular deficit of the NMJs on slow myofibers.

NMJs in Albino EOMs Did Not Show the Normal Increase in Size in Early Postnatal Development

Although we did not find a difference in NMJ size in adults, we examined NMJ size during postnatal development. In control EOMs, there was an increase in NMJ size between P0 and P10, then a gradual decrease in size. In albinos, this increase did not occur, leading to significantly smaller NMJs at P10 and P14 but not at other ages (Figs. 5A, 5D). Together, these findings suggest that there are NMJ structural developments that occur normally in early postnatal development that are not occurring in albinos.

Discussion

We demonstrated that Balb/c albino mice with nystagmus have changes in EOM myofiber subtype and innervation similar to those previously seen in human samples, providing further evidence that they are a good model for studying the pathophysiology of nystagmus. We further demonstrate that the onset of changes in EOMs and their innervation is during the second postnatal week in albino mice, with the earliest changes (in NMJ density) evident as early as P10, before eye opening in mice.

Relatively little is known about the underlying pathophysiology of INS. Because afferent visual dysfunction of many different types is associated with INS, it has been theorized that there is vision-dependent control of the oculomotor system, the disruption of which leads to nystagmus. It was not known whether the EOM abnormalities reported in humans with nystagmus were the cause or the effect of long-standing nystagmus. We show here, however, that EOM changes are first evident in early postnatal development in a mouse model. In albino mice, there are underlying abnormalities of EOM innervation even before eye opening which cannot be caused by poor vision. There are likely other aspects of oculomotor development that are influenced by poor vision, but we provide evidence that INS, at least in albinos, may not solely be secondary to poor vision. The age of onset of nystagmus in mice is not known and cannot be determined with currently available methods, but we presume it is not before eye opening.

Balb/c mice have the Tyr^c point mutation in tyrosinase, which causes a cysteine-to-serine mutation at amino acid 103.[24] These mice have no tyrosinase activity and thus no melanin in their pigment cells, but the pigment cells are present.[15] Although the mutation eliminates tyrosinase activity, the gene is expressed normally.[25] In mice, *Tyr* expression is limited to two cell types—retinal pigment epithelium and neural crest derived melanocytes (which migrate during development to multiple areas of the body, including skin, hair bulbs, choroid, and cochlea.)[26] Expression in the retinal pigment epithelium begins at E10.5 and in skin melanocytes at E16.5.[25] *Tyr* is not expressed in developing or adult brain.[27]

In both skeletal muscles and EOMs, at birth myofibers transiently receive multiple motor neuron axon terminals on end plates (postsynaptic sites) and during the second postnatal week most of these terminals retract, resulting in single innervation on fast myofibers.[28–30] The loss of the axon terminals also causes the pruning of postsynaptic sites on the myofibers (i.e., AChRs).[29,31] The decrease in NMJ density between P0 and P10 is more pronounced in albino mice, suggesting that there may be excessive pruning of the nerve terminals.

In skeletal muscles, it has been reported that the neuromuscular junctions are simple structures at P7, which expand into complex, branched AChR clusters and become mature by P21.[28] During the second postnatal week, NMJ reorganization takes place by stabilizing the AChRs, forming subsynaptic infoldings of membrane, and recruiting muscle nuclei beneath the postsynaptic membrane.[32,33] We found that NMJ size on EOMs increases between P10 and P14 in control animals but not in albinos, suggesting that NMJs are not maturing properly. Abnormal development of the NMJs may affect efficiency of synaptic transmission or postsynaptic receptor stability and signaling and thus the trophic support provided to muscles by their innervating neurons

Investigative Ophthalmology & Visual Science

Downloaded from intl.iovs.org on 04/26/2024

(see below). In humans, decreased NMJ size in nystagmus samples was seen in a mixed population of children and adults, whereas in mice we found only a developmental change, with normal NMJ size in adulthood. This may reflect differences in NMJ maturation between the species or may be because the population of humans studied varied in age. Tyrosinase is not expressed in developing motor neurons or in EOMs.[27] Precisely how the absence of tyrosinase activity leads to abnormalities of NMJ development will require further study.

Albino mice EOMs also display a shift of muscle fiber type toward slow myofibers in both the orbital and global layers, despite underlying differences in slow myofiber percentages between the layers.[34] Changes in myofiber type composition in skeletal muscles have been seen in neurodegenerative mouse models[35,36] and in muscle atrophy.[37] Muscle atrophy associated with denervation and immobilization is associated with slow-to-fast fiber-type shifts, whereas atrophy associated with fasting, cachexia, and aging is associated with fast-to-slow fiber-type shifts.[37] In skeletal muscles, muscle fiber type specification is regulated by trophic factors, including brain-derived neurotrophic factor (BDNF), which modulates the shift from fast to slow myofibers and AChR disassembly.[38,39] Muscle fiber-type specification is also influenced by a variety of miRNAs, muscle-derived proteins, and membrane proteins.[40–43] Several studies have reported that muscle-derived neurotrophic factors provide retrograde signals to motor neurons and are required for NMJ development, maintenance, and remodeling.[38,39,42,44,45] VEGF blockade at the lateral rectus causes reductions in the firing rate, sensitivity, and afferent synaptic inputs in abducens motoneurons, similar to those seen with axotomy.[46] After axotomy, retrograde delivery of VEGF restores these parameters.[47] Interestingly, EOMs from humans with albinism show low levels of BDNF expression,[13] suggesting a role for BDNF in NMJ development and EOM specification.

NMJ density and size differences between albinos and controls are present earlier than are the changes in proportion of myofiber subtypes, suggesting that changes in innervation may influence myofiber subtype specification. Slow and fast myofibers are innervated by different types of motor neurons, which have different function properties.[8,10,11,48] EOMs and OMNs are dependent on each other for trophic support. Muscle-derived cues promote OMN survival,[49] and cell death significantly increases in the absence of normal muscle targets,[19] consistent with the theory that muscles provide trophic support for developing motor neurons.[50] EOMs also influence axon guidance during early development.[19,22,51] How motor neuron subtypes are matched with the proper myofiber subtype is not fully understood, although there is evidence in skeletal muscles of a retrograde influence of myofiber subtype on motor neuron specification.[44] An imbalance in the proportion of slow and fast motor neurons or abnormalities in NMJ development of one type of OMN could underlie the differences in proportions of myofiber subtypes seen in albinos. The data from humans with nystagmus were collected before the discovery of a novel type of multiterminal motor endplate in human EOMs, which is present on myofibers that do not express fast or slow MyHC but instead express the EOM-specific form of MyHC.[52] It is therefore unknown whether this type of myofiber is altered in nystagmus. In mice, we found myofibers that do not express slow or fast myosin in high numbers at P0 and a much lower percentage at older ages. At no age was there a difference between control and albino in these negative fibers.

In conclusion, we have shown here that EOMs from albino mice show the same changes in EOM subtype proportion and NMJ density as seen in human patients with nystagmus. Furthermore, we have shown that the NMJ changes are present as early as P10, before eye opening and presumably before the onset of nystagmus. Our findings indicate that there are primary abnormalities of EOM innervation that are not secondary to poor vision, contributing to the development of nystagmus in albinism. Further studies are needed to investigate how the absence of tyrosinase activity leads to abnormalities of NMJ development, whether the change in the proportion of muscle fiber type occurs because of changes in the proportion of SIF- and MIF-innervating neurons, and whether these results are true in other causes of INS.

Acknowledgments

The authors thank the Massachusetts Lions Eye Research Fund, Boston Children's Hospital Faculty Development Award, Children's Hospital Ophthalmology Foundation, Boston Children's Hospital Translational Research Program, and the Malik Family Fund for financial support.

Disclosure: **S.K. Vemula**, None; **S.A. Kim**, None; **T. Muvavarirwa**, None; **J.L. Bell**, None; **M.C. Whitman**, None

References

1. Nash DL, Diehl NN, Mohney BG. Incidence and types of pediatric nystagmus. *Am J Ophthalmol*. 2017;182:31–34.
2. Abadi RV, Bjerre A. Motor and sensory characteristics of infantile nystagmus. *Br J Ophthalmol*. 2002;86:1152–1160.
3. Winkelman BHJ, Howlett MHC, Holzel MB, et al. Nystagmus in patients with congenital stationary night blindness (CSNB) originates from synchronously firing retinal ganglion cells. *PLoS Biol*. 2019;17:e3000174.
4. Whitman MC. Axonal growth abnormalities underlying ocular cranial nerve disorders. *Annu Rev Vis Sci*. 2021;7:827–850.
5. Porter JD. Extraocular muscle: cellular adaptations for a diverse functional repertoire. *Ann N Y Acad Sci*. 2002;956:7–16.
6. Bormioli SP, Torresan P, Sartore S, Moschini GB, Schiaffino S. Immunohistochemical identification of slow-tonic fibers in human extrinsic eye muscles. *Invest Ophthalmol Vis Sci*. 1979;18:303–306.
7. Khanna S, Richmonds CR, Kaminski HJ, Porter JD. Molecular organization of the extraocular muscle neuromuscular junction: Partial conservation of and divergence from the skeletal muscle prototype. *Invest Ophthalmol Vis Sci*. 2003;44:1918–1926.
8. Buttner-Ennever JA, Horn AK, Scherberger H, D'Ascanio P. Motoneurons of twitch and nontwitch extraocular muscle fibers in the abducens, trochlear, and oculomotor nuclei of monkeys. *J Comp Neurol*. 2001;438:318–335.
9. Ugolini G, Klam F, Doldan Dans M, et al. Horizontal eye movement networks in primates as revealed by retrograde transneuronal transfer of rabies virus: differences in monosynaptic input to "slow" and "fast" abducens motoneurons. *J Comp Neurol*. 2006;498:762–785.
10. Carrero-Rojas G, Hernandez RG, Blumer R, de la Cruz RR, Pastor AM. MIF versus SIF motoneurons, what are their

Investigative Ophthalmology & Visual Science

Downloaded from intl.iovs.org on 04/26/2024

respective contribution in the oculomotor medial rectus pool? *J Neurosci*. 2021;41:9782–9793.
11. Hernandez RG, Calvo PM, Blumer R, de la Cruz RR, Pastor AM. Functional diversity of motoneurons in the oculomotor system. *Proc Natl Acad Sci USA*. 2019;116:3837–3846.
12. Berg KT, Hunter DG, Bothun ED, Antunes-Foschini R, McLoon LK. Extraocular muscles in patients with infantile nystagmus: adaptations at the effector level. *Arch Ophthalmol*. 2012;130:343–349.
13. McLoon LK, Willoughby CL, Anderson JS, et al. Abnormally small neuromuscular junctions in the extraocular muscles from subjects with idiopathic nystagmus and nystagmus associated with albinism. *Invest Ophthalmol Vis Sci*. 2016;57:1912–1920.
14. Traber GL, Chen CC, Huang YY, et al. Albino mice as an animal model for infantile nystagmus syndrome. *Invest Ophthalmol Vis Sci*. 2012;53:5737–5747.
15. Coleman DL. Effect of genic substitution on the incorporation of tyrosine into the melanin of mouse skin. *Arch Biochem Biophys*. 1962;96:562–568.
16. Lewcock JW, Genoud N, Lettieri K, Pfaff SL. The ubiquitin ligase Phr1 regulates axon outgrowth through modulation of microtubule dynamics. *Neuron*. 2007;56:604–620.
17. Renier N, Adams EL, Kirst C, et al. Mapping of brain activity by automated volume analysis of immediate early genes. *Cell*. 2016;165:1789–1802.
18. Whitman MC, Nguyen EH, Bell JL, Tenney AP, Gelber A, Engle EC. Loss of CSCR4/CSCL12 signaling causes oculomotor nerve misrouting and development of motor trigeminal to oculomotor synkinesis. *Invest Ophthalmol Vis Sci*. 2018;59:5201–5209.
19. Michalak SM, Whitman MC, Park JG, Tischfield MA, Nguyen EH, Engle EC. Ocular motor nerve development in the presence and absence of extraocular muscle. *Invest Ophthalmol Vis Sci*. 2017;58:2388–2396.
20. Nugent AA, Park JG, Wei Y, et al. Mutant α2-chimaerin signals via bidirectional ephrin pathways in Duane retraction syndrome. *J Clin Invest*. 2017;127:1664–1682.
21. Whitman MC, Miyake N, Nguyen EH, et al. Decreased ACKR3 (CSCR7) function causes oculomotor synkinesis in mice and humans. *Hum Mol Genet*. 2019;28:3113–3125.
22. Bjorke B, Weller KG, Jones LE, et al. Oculomotor nerve guidance and terminal branching requires interactions with differentiating extraocular muscles. *Dev Biol*. 2021;476:272–281.
23. Zhou Y, Liu D, Kaminski HJ. Myosin heavy chain expression in mouse extraocular muscle: more complex than expected. *Invest Ophthalmol Vis Sci*. 2010;51:6355–6363.
24. Yokoyama T, Silversides DW, Waymire KG, Kwon BS, Takeuchi T, Overbeek PA. Conserved cysteine to serine mutation in tyrosinase is responsible for the classical albino mutation in laboratory mice. *Nucleic Acids Res*. 1990;18:7293–7298.
25. Beermann F, Schmid E, Schutz G. Expression of the mouse tyrosinase gene during embryonic development: recapitulation of the temporal regulation in transgenic mice. *Proc Natl Acad Sci USA*. 1992;89:2809–2813.
26. Seruggia D, Josa S, Fernandez A, Montoliu L. The structure and function of the mouse tyrosinase locus. *Pigment Cell Melanoma Res*. 2021;34:212–221.
27. Gimenez E, Lavado A, Giraldo P, Montoliu L. Tyrosinase gene expression is not detected in mouse brain outside the retinal pigment epithelium cells. *Eur J Neurosci*. 2003;18:2673–2676.
28. Fox MA, Tapia JC, Kasthuri N, Lichtman JW. Delayed synapse elimination in mouse levator palpebrae superioris muscle. *J Comp Neurol*. 2011;519:2907–2921.
29. Lichtman JW, Colman H. Synapse elimination and indelible memory. *Neuron*. 2000;25:269–278.
30. Tapia JC, Wylie JD, Kasthuri N, et al. Pervasive synaptic branch removal in the mammalian neuromuscular system at birth. *Neuron*. 2012;74:816–829.
31. Balice-Gordon RJ, Lichtman JW. In vivo observations of pre- and postsynaptic changes during the transition from multiple to single innervation at developing neuromuscular junctions. *J Neurosci*. 1993;13:834–855.
32. Tintignac LA, Brenner HR, Ruegg MA. Mechanisms regulating neuromuscular junction development and function and causes of muscle wasting. *Physiol Rev*. 2015;95:809–852.
33. Lee YI. Differences in the constituent fiber types contribute to the intermuscular variation in the timing of the developmental synapse elimination. *Sci Rep*. 2019;9:8694.
34. Spencer RF, Porter JD. Biological organization of the extraocular muscles. *Prog Brain Res*. 2006;151:43–80.
35. Palamiuc L, Schlagowski A, Ngo ST, et al. A metabolic switch toward lipid use in glycolytic muscle is an early pathologic event in a mouse model of amyotrophic lateral sclerosis. *EMBO Mol Med*. 2015;7:526–546.
36. Dobrowolny G, Lepore E, Martini M, et al. Metabolic changes associated with muscle expression of $SOD1^{G93A}$. *Front Physiol*. 2018;9:831.
37. Dumitru A, Radu BM, Radu M, Cretoiu SM. Muscle changes during atrophy. *Adv Exp Med Biol*. 2018;1088:73–92.
38. Delezie J, Weihrauch M, Maier G, et al. BDNF is a mediator of glycolytic fiber-type specification in mouse skeletal muscle. *Proc Natl Acad Sci USA*. 2019;116:16111–16120.
39. Gonzalez M, Ruggiero FP, Chang Q, et al. Disruption of Trkb-mediated signaling induces disassembly of postsynaptic receptor clusters at neuromuscular junctions. *Neuron*. 1999;24:567–583.
40. Quiat D, Voelker KA, Pei J, et al. Concerted regulation of myofiber-specific gene expression and muscle performance by the transcriptional repressor sox6. *Proc Natl Acad Sci USA*. 2011;108:10196–10201.
41. Chalkiadaki A, Igarashi M, Nasamu AS, Knezevic J, Guarente L. Muscle-specific SIRT1 gain-of-function increases slow-twitch fibers and ameliorates pathophysiology in a mouse model of Duchenne muscular dystrophy. *PLoS Genet*. 2014;10:e1004490.
42. Correia JC, Kelahmetoglu Y, Jannig PR, et al. Muscle-secreted neurturin couples myofiber oxidative metabolism and slow motor neuron identity. *Cell Metab*. 2021;33:2215–2230.e8.
43. Zhang D, Wang X, Li Y, et al. Thyroid hormone regulates muscle fiber type conversion via miR-133a1. *J Cell Biol*. 2014;207:753–766.
44. Chakkalakal JV, Nishimune H, Ruas JL, Spiegelman BM, Sanes JR. Retrograde influence of muscle fibers on their innervation revealed by a novel marker for slow motoneurons. *Development*. 2010;137:3489–3499.
45. Morcuende S, Munoz-Hernandez R, Benitez-Temino B, Pastor AM, de la Cruz RR. Neuroprotective effects of NGF, BDNF, NT-3 and GDNF on axotomized extraocular motoneurons in neonatal rats. *Neuroscience*. 2013;250:31–48.
46. Calvo PM, Hernandez RG, de la Cruz RR, Pastor AM. VEGF is an essential retrograde trophic factor for motoneurons. *Proc Natl Acad Sci USA*. 2022;119:e2202912119.
47. Calvo PM, de la Cruz RR, Pastor AM. Synaptic loss and firing alterations in axotomized motoneurons are restored by vascular endothelial growth factor (VEGF) and VEBF-B. *Exp Neurol*. 2018;304:67–81.
48. Wasicky R, Horn AK, Buttner-Ennever JA. Twitch and nontwitch motoneuron subgroups in the oculomotor nucleus of monkeys receive different afferent projections. *J Comp Neurol*. 2004;479:117–129.
49. Rind HB, von Bartheld CS. Target-derived cardiotrophin-1 and insulin-like growth factor-i promote neurite growth

Investigative Ophthalmology & Visual Science

Downloaded from intl.iovs.org on 04/26/2024

and survival of developing oculomotor neurons. *Mol Cell Neurosci*. 2002;19:58–71.

50. Benítez-Temino B, Davis-López de Carrizosa MA, Morcuende S, Matarredona ER, de la Cruz RR, Pastor AM. Functional diversity of neurotrophin actions on the oculomotor system. *Int J Mol Sci*. 2016;17: 2016.
51. Munezane H, Oizumi H, Wakabayashi T, et al. Roles of collagen XXV and its putative receptors PTPσ/δ in intramuscular motor innervation and congenital cranial dysinnervation disorder. *Cell Rep*. 2019;29:4362–4376.e6.
52. Liu JX, Domellof FP. A novel type of multiterminal motor endplate in human extraocular muscles. *Invest Ophthalmol Vis Sci*. 2018;59:539–548.

Investigative Ophthalmology & Visual Science

Downloaded from intl.iovs.org on 04/26/2024